ACS APPLIED MATERIALS & INTERFACES

Research Article

www.acsami.org

# High Photoresponsivity and Short Photoresponse Times in Few-Layered $WSe_2$ Transistors

Nihar R. Pradhan,*[,†] Jonathan Ludwig,[†,‡] Zhengguang Lu,[†,‡] Daniel Rhodes,[†,‡] Michael M. Bishop,[†] Komalavalli Thirunavukkuarasu,[†] Stephen A. McGill,[†] Dmitry Smirnov,[†] and Luis Balicas*[,†,‡]

[†]National High Magnetic Field Lab, Florida State University, 1800 E. Paul Dirac Drive, Tallahassee, Florida 32310, United States

[‡]Department of Physics, Florida State University, Tallahassee, Florida 32306, United States

Supporting Information

**ABSTRACT:** Here, we report the photoconducting response of field-effect transistors based on three atomic layers of chemical vapor transport grown $WSe_2$ crystals mechanically exfoliated onto $SiO_2$. We find that trilayered $WSe_2$ field-effect transistors, built with the simplest possible architecture, can display high hole mobilities ranging from 350 $cm^2/(V\,s)$ at room temperature (saturating at a value of ~500 $cm^2/(V\,s)$ below 50 K) displaying a strong photocurrent response, which leads to exceptionally high photoresponsivities up to 7 A/W under white light illumination of the entire channel for power densities $p < 10^2$ $W/m^2$. Under a fixed wavelength of $\lambda = 532$ nm and a laser spot size smaller than the conducting channel area, we extract photoresponsitivities approaching 100 mA/W with concomitantly high external quantum efficiencies up to ~40% at room temperature. These values surpass values recently reported from more complex architectures, such as graphene and transition metal dichalcogenides based heterostructures. Also, trilayered $WSe_2$ phototransistors display photoresponse times on the order of 10 $\mu$s. Our results indicate that the addition of a few atomic layers considerably decreases the photoresponse times, probably by minimizing the interaction with the substrates, while maintaining a very high photoresponsivity.

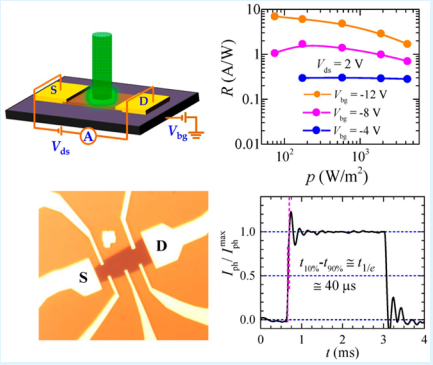


**KEYWORDS:** *two-dimensional atomic layers, transition metal dichalcogenides, tungsten diselenide, field-effect transistors, photocurrent, quantum efficiency*

## INTRODUCTION

Although graphene[1] is the most studied two-dimensional, or layered material, single or few atomic layers of other van der Waals solids, such as insulating *h*-BN[2] or semiconducting transition metal dichalcogenides (TMDs) such as $MoS_2$,[3,4] $MoSe_2$[5−7] or $WSe_2$,[8,9] are being intensively investigated, as either promising gate dielectrics or as the conducting channel material in field-effect transistors (FETs). Because monolayer $MoS_2$ has been shown to be a direct-bandgap semiconductor,[10,11] due to quantum-mechanical confinement,[10,12,13] it was suggested that it could be a suitable material for optoelectronic applications[14] where the direct bandgap would naturally lead to a high absorption coefficient and therefore to efficient electron−hole pair generation under photoexcitation. Its potential for applicability is further supported by the overall behavior of the FETs, which display high ON to OFF current ratios, i.e., up to $10^8$,[4] photogains as high as 5000[15] and high specific detectivities, i.e., up to $10^{10}$−$10^{11}$ Jones.[16]

However, the photoresponse of single-layer $MoS_2$ is a matter of controversy, with reports indicating either the absence of a sizable response[16,17] or, and in contrast, a high photocurrent when the phototransistor is its "ON" state.[14,18−20] Most reports attribute the observed photocurrent to the separation of photogenerated electron and hole pairs at the interface between the semiconductor and the metallic electrical contact[14−20] although others claim a prominent role for the photothermoelectric effect (resulting from the difference in the Seebeck coefficients between the contact and the channel materials and the presence of light-induced temperature gradients).[21] The Schottky barriers between the semiconducting channel and the metallic electrodes, which result from the difference between the electron affinity of the semiconductor and the work function of the metal, are expected to play a major role in any conventional photodetector.[22] Several groups tentatively attributing the differences among the observed electrical and/or optical transport properties, to the size of the Schottky barrier.[15,18,21] In addition, the bending of the conduction and valence bands in the vicinity of the metallic contacts, which leads to pronounced local electric fields under a bias voltage, were claimed to contribute significantly to photocurrent generation.[20]

The electrical contacts would also play a relevant role for the photoconducting temporal response. It is reported to vary widely from characteristic rising/decay times inferior to a 1 ms

Received: March 14, 2015
Accepted: May 19, 2015
Published: May 19, 2015





DOI: 10.1021/acsami.5b02264
ACS Appl. Mater. Interfaces 2015, 7, 12080−12088

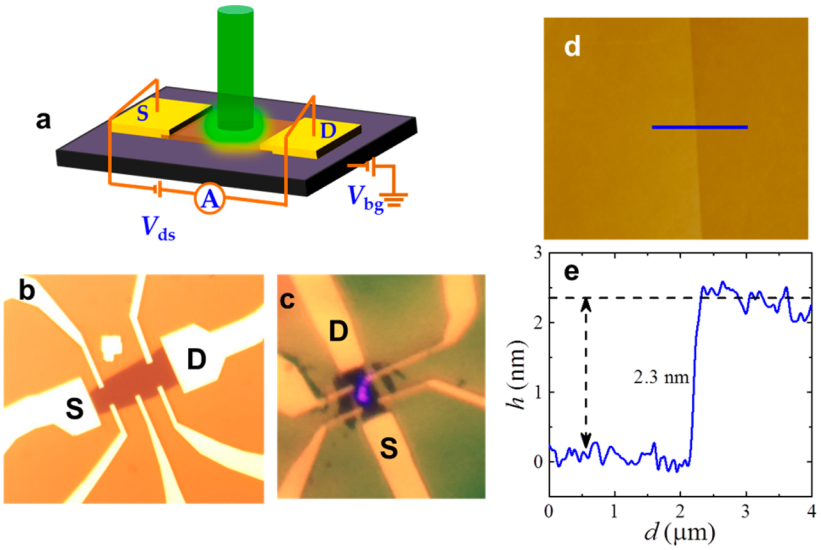


**Figure 1.** (a) Sketch of our experimental setup showing drain (D) and source (S) current electrodes. Green cylinder depicts the laser beam, whose spot size is chosen to be considerably smaller than the active $WSe_2$ channel area to minimize the interaction with the charge carriers flowing through the current leads. (b) Micrograph of one of our trilayered $WSe_2$ based field-effect transistors, indicating electrical current pads, as well as electrical connections for four-terminal resistivity and Hall-effect measurements. This sample of channel length $l$ = 22.22 $\mu$m and an average width $w$ = 8.37 $\mu$m was mainly used for two-terminal electrical transport measurements. Here "S" and "D" denote source and drain contacts, respectively. (c) Micrograph of a second trilayered $WSe_2$ field-effect transistor. This sample of channel length $l$ = 15.8 $\mu$m and an average width $w$ = 8.6 $\mu$m was mainly used for evaluating the photoconducting response. As seen, a violet laser spot is shone onto the channel. (d) Atomic force microscopy image along the edge of the sample in panel c. Blue line indicates the line along which the height profile (shown in panel e) was collected. The height profile indicates a step of 2.3 nm or 3 atomic layers (each with a thickness of 0.647 nm).

to values surpassing 30 s, for either mechanically exfoliated or chemical vapor deposited (CVD) $MoS_2$.[15−18] For instance, phototransistors based on large-area, CVD synthesized, $WSe_2$ monolayers electrically contacted with Pd, which presumably display small Schottky barriers, are found to exhibit high photogain ($10^5$) and specific detectivity ($10^{14}$ Jones), but with characteristic response times >5 s in air.[23] In contrast, when these phototransistors are contacted with Ti, which is claimed to lead to a higher Schottky barrier, they would display a fast response time, i.e., shorter than 23 ms, but with several orders of magnitude lower photogain and specific detectivity.[23]

Here, we explore the photoresponse properties of field-effect transistors based on three atomic layers of $WSe_2$ exfoliated onto $SiO_2$:$p$-Si substrates contacted with a single combination of Ti:Au contacts. We find large photoresponsivities approaching 7 A/W (under white light and for illumination power densities $10 < p < 10^2$ W/m$^2$) and external quantum efficiencies approaching 40% (under laser illumination at $\lambda$ = 532 nm). These values can still increase considerably by varying either the bias or the back gate voltages or both, and/or simply by illuminating the whole area of the conducting channel. Their characteristic response time is found to remain within a few tenths of microseconds. Improvements in the quality of the electrical contacts, the starting materials and substrates is likely to improve their performance making few-layer $WSe_2$ phototransistors potentially useful for optoelectronics applications.

## RESULTS AND DISCUSSION

Figure 1a shows a schematic of our multilayered $WSe_2$ based field-effect transistors and the configuration of measurements. The devices are composed of three atomic layers of $WSe_2$, which are electrically contacted by using a combination of Ti and Au. Figure 1b shows a micrograph of one of our trilayered $WSe_2$ FETs whose detailed electrical transport characterization is presented in the Supporting Information and which will be briefly discussed below. As seen in Figure 1c, the spot size of the laser beam (3.5 $\mu$m) was intentionally chosen to be smaller than the area of the conducting channel in order to minimize the interaction with the area surrounding the electrical contacts. Figures 1d displays an atomic force microscopy (AFM) image of the edge of the $WSe_2$ from which we extracted the height profile shown in Figure 1e.

Our trilayered $WSe_2$ FETs behave as hole-doped transistors, i.e., yielding a sizable current (on the order of 1 $\mu$A/$\mu$m at low excitation voltages $V_{ds}$) only for negative gate voltages $V_{bg}$ surpassing a certain threshold value $V_{bg}^t$, see Figure 2. The ON to OFF ratio surpasses $10^6$ but with relatively large subthreshold swings SS ≅ 5 V. The room temperature values of $V_{bg}^t$ are sample dependent varying from −30 and −40 V, and increasing as the temperature is lowered, as can be seen by comparing Figures 2a and c and b and d. This behavior is attributable to disorder-induced carrier localization in the channel as extensively studied in $Si/SiO_2$ MOSFETs.[24] Above $V_{bg}^t$ and from the slopes of $I_{ds}$ as a function of $V_{bg}$, and by applying the MOSFET transconductance formula, $\mu_{Fe} = 1/c_g d\sigma/dV_{bg}$, where $\sigma = I_{ds}\, l/V_{ds}\, w$ with $l$ and $w$ being the length and the width of the channel respectively, and $c_g = \varepsilon_r\varepsilon_0/d$ = 12.789 × $10^{-9}$ F/cm$^2$ for a $d$ = 270 nm thick $SiO_2$ layer, we obtain maximum two-terminal field-effect hole mobilities exceeding $\mu_{FE}$ ≅ 350 cm$^2$/(V s) at $T$ = 275 K. $\mu_{FE}$ increases to values surpassing ∼500 cm$^2$/(V s) at $T$ = 20 K due to the suppression of phonon scattering, see also Figure S1 of the Supporting Information. These near room-temperature values for the two-terminal field-effect mobilities are considerably higher than the ones extracted for electron-doped multilayered $MoS_2$ FETs.[25] This suggests that our chemical vapor transport synthesized $WSe_2$ single-crystals are less disordered than natural $MoS_2$. Our extracted mobilities are higher than those


DOI: 10.1021/acsami.5b02264
ACS Appl. Mater. Interfaces 2015, 7, 12080−12088

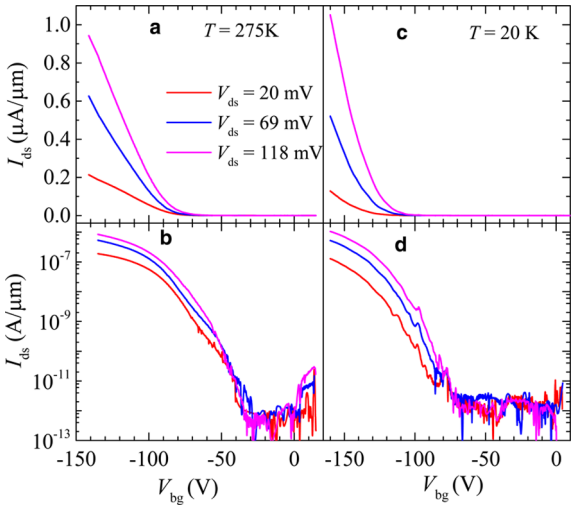


**Figure 2.** (a) Source to drain current $I_{ds}$ normalized by the width $w$ of the channel as a function of the back gate voltage $V_{bg}$ and for several values of drain-source excitation voltage $V_{ds}$ of 20 (red line), 69 (blue line) and 118 mV (magenta line), respectively. As seen a sizable current $I_{ds}$ is observed only for negative values of $V_{bg}$, indicating hole-conduction once the $V_{bg}$ surpasses a threshold value. (b) Same as in panel a but in a logarithmic scale. (c) Same as in panel a (including excitation voltages and respective line colors) but at a temperature $T$ = 20 K. (d) Same as in panel c but in a logarithmic scale.

obtained at $T$ = 80 K for encapsulated multilayered $WSe_2$ using graphene for the electrical contacts and ionic liquid gating[26] but close to the value of ~600 $cm^2/(V\ s)$ extracted also for ionic liquid gated and $h$-BN encapsulated multilayered $WSe_2$ at $T$ = 220 K.[27] Insofar, the highest room temperature mobility reported for multilayered $WSe_2$, i.e., ~500 $cm^2/(V\ s)$, was obtained by using parylene as the gate dielectric.[28] On $SiO_2$, we obtained $\mu_{FE} \sim 350\ cm^2/(V\ s)$ at $T$ = 300 K for crystals composed of approximately 10 atomic layers, and whose value increased up to ~670 $cm^2/(V\ s)$ at $T$ = 105 K.[29] Most importantly, in these samples, we found a broad agreement between field-effect and Hall mobilities, with their difference ascribed to an underestimation of the value of the gate capacitance used in the transconductance formula, most likely due to the presence of spurious charges.[29] The gate-induced decrease in the size of the Schottky barriers at the contacts and the screening of both impurities and charge carriers in the neighborhood of the mobility edge should contribute to higher field-effect mobilities.

As discussed above, the metallic electrical contacts were claimed to play a major role in the photoconducting response of FETs based on TMDs; therefore, we proceed to analyze the quality of our Au (~90 nm) on Ti (~4 nm) contacts and evaluate the size of the Schottky barriers. As seen in Figure 3a at low excitation voltages $V_{ds}$, the drain to source current $I_{ds}$ is linear (or ohmic like) in $V_{ds}$, independently of the applied back gate-voltage $V_{bg}$. This indicates that any Schottky barrier between $WSe_2$ and the contacts plays a quite mild role at room temperature, with carriers being promoted across the barrier by thermionic emission or thermionic field emission processes.[30,31] In effect, according to thermionic emission theory,[30,31] the drain to source current $I_{ds}$ is related to the Schottky barrier height $\phi_{SB}$ through the expression:

$$I \cong AA^*T^2 \exp\left(\frac{e\phi_{SB}}{k_BT}\right)\left[1 - \exp\left(-\frac{eV_{ds}}{k_BT}\right)\right] \quad (1)$$

where, $A$ is the area of the Schottky junction, $A^* = 4\pi em^*k_B^2h^{-3}$ is the effective Richardson constant, $e$ is the elementary charge, $k_B$ is the Boltzmann constant, $m^*$ is the effective mass and $h$ is the Planck constant. To evaluate the Schottky barrier at the level of the contacts, in Figure 3c, we plot $I_{ds}$ normalized by the square of the temperature $T^2$ as a function of $e/k_BT$ and for several values of $V_{bg}$. Linear fits, depicted by straight lines from which we extract $\phi_{SB}$, are limited

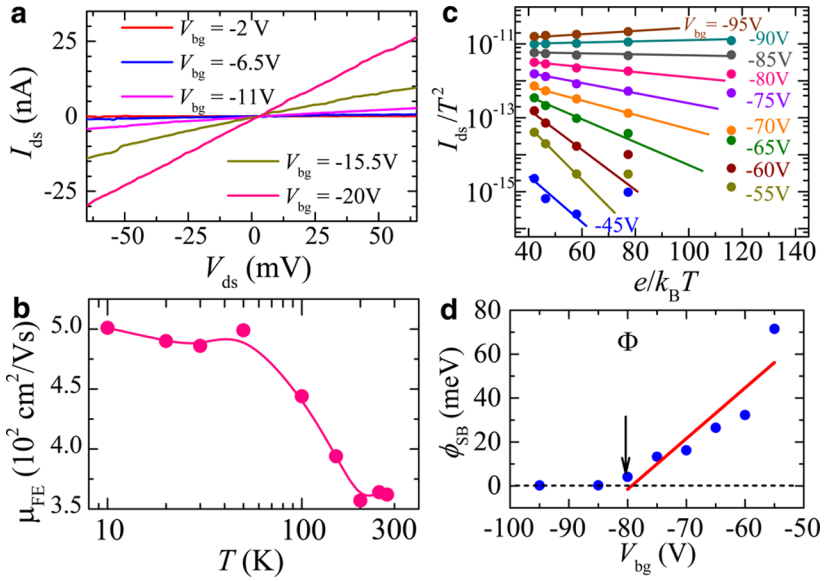


**Figure 3.** (a) Drain to source current $I_{ds}$ as a function of the excitation voltage $V_{ds}$ for several values of the gate voltage $V_{bg}$. Linear dependence at low excitation voltages indicates a small role for the Schottky barriers. (b) Field effect mobility $\mu_{FE}$ as a function of the temperature $T$, as calculated from the curves in Figure S2 of the Supporting Information. For this trilayered sample, $\mu_{FE}$ saturates at ~500 $cm^2/(V\ s)$ at low $T$'s. (c) $I_{ds}$ normalized by the square of the temperature $T^2$ as a function of $e/k_BT$, where $e$ is the electron charge and $k_B$ is the Boltzmann constant. (d) $\phi_{SB}$ as a function of $V_{bg}$. Red line is a linear fit. Deviations from linearity are observed above $V_{bg} \cong -80$ V, suggesting a rather small Shottky barrier of just a few meV.


DOI: 10.1021/acsami.5b02264
ACS Appl. Mater. Interfaces 2015, 7, 12080−12088

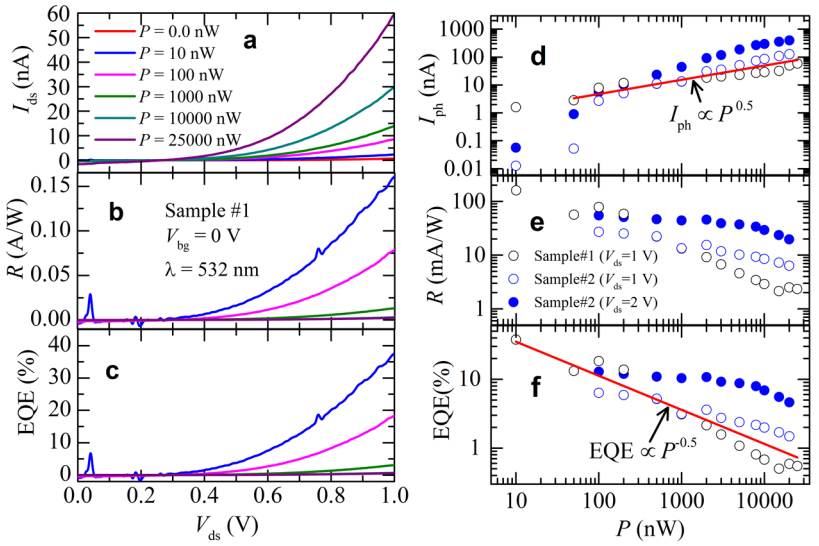


**Figure 4.** (a) Drain to source current $I_{ds}$ as a function of bias voltage $V_{ds}$ for a trilayered $WSe_2$ field effect transistor under zero gate voltage ($V_{bg}$ = 0 V) and for several values of the optical power (for a wavelength $\lambda$ = 532 nm). (b) Photoresponsivity $R = I_{ph}/P$, where $I_{ph} = (I_{ds}(P) - I_{ds}(P = 0))$, as a function of $V_{ds}$. (c) Resulting external quantum efficiency (EQE) as a function of $V_{ds}$. (d) $I_{ph}$ as a function of the applied optical power $P$ in a log–log scale and for two samples, where open circles depict $I_{ph}(V_{ds}$ = 1 V), and closed ones $I_{ph}$ for $V_{ds}$ = 2 V (sample #2). Red line is a power law fit indicating an exponent $\alpha$ = 0.5, or that $I_{ph}$ tends to saturate at high $P$ levels, likely due to an increased role for exciton recombination processes. (e) Photoresponsivity as a function of laser power, $R(P)$, from the data in panel d, indicating that $R$ reaches values as high as, or exceeds 100 mA/W at low $P$ levels, but decreases by several orders of magnitude as $P$ increases. (f) EQE as a function of $P$, in a log–log scale from the data in panel e. (f) Red line is a linear fit yielding an exponent $\alpha$ = −0.5.

to higher temperatures because at lower $T$'s, one observes pronounced gate dependent deviations from linearity. Figure 3d shows $\phi_{SB}$ as a function of $V_{bg}$ where the red line is a linear fit. From the deviation from linearity (the so-called flat band condition) one extracts the size of the Schottky barrier $\Phi$.[31] A pronounced deviation from linearity is observed beyond $V_{bg} \cong -80$ V, where the size of $\Phi$ is of just a few meV, indicating a better band alignment than what is a priori expected from the difference between the work function of Ti (4.33 eV) and the electron affinity of $WSe_2$ (≅4.00 eV).[32] Therefore, Ti would seem to lead to a small Schottky barrier in contrast to the claims of ref 23. The use of a different temperature prefactor, i.e., $T^{\alpha}$ with $\alpha$ = 1.5 or 1 but ≠2 yields similar results. This small $\Phi$ value might result from defects and impurities[33] around the contact area which would pin the Fermi level at an arbitrary position relative to the conduction and valence bands. Or it might result from thermally assisted tunneling through a quite thin Schottky barrier.

Having clarified this aspect, we now return to the issue of carrier localization due to the disorder in the channel. In Figure S2 of the Supporting Information, we plot the two-terminal conductivity $\sigma$ as a function of $T^{-1/3}$, the dependence expected for the two-dimensional variable range hopping conductivity mechanism. We find that it perfectly describes the data on a broad range of temperatures and gate voltages, but particularly at lower gate voltages, as previously seen by other groups working on FETs based on TMDs.[34,35] We ascribe the threshold back gate voltage $V_{bg}^{t}$ to the existence of a mobility edge. Atomic level roughness, dangling bonds, and buried charges, for example from Na treatment of the $SiO_2$ layer, create a random Coulomb potential on the $SiO_2$ substrate, contributing to disorder, which leads to carrier localization. Dislocations in the TMD layers,[34,35] adsorbates and residues from the fabrication process also contribute to disorder and hence to localization. The initial accumulation of charges in the channel through the field-effect contributes to the screening of spurious charges, which act as traps for charge carriers. Additional carriers accumulated into the channel become mobile and yield sizable currents only when these traps are fully screened, or when $V_{bg} > V_{bg}^{t}$. $V_{bg}^{t}$ is temperature-dependent because at higher temperatures, thermal activated processes would contribute to carrier detrapping and hence would decrease the values of $V_{bg}^{t}$, as seen experimentally. At the moment, we do not have a detailed understanding on the nature and on the role of disorder in these systems, but our experimental results are unambiguous.

Next, we proceed to evaluate phototransport properties of our trilayered $WSe_2$ FETs under coherent light illumination. The transition toward a direct band gap is predicted to occur, and has indeed been observed in single atomic layers of TMDs.[14] Hence, in monolayers, illumination leads to the efficient creation of electron–hole pairs because it does not require the intervention of phonons. Nevertheless, we chose to work with trilayered devices for two reasons: (i) similarly to the motivation for fabricating $h$-BN encapsulated samples,[26,27] one would expect the top atomic-layer to act as a capping layer, thus minimizing the role of adsorbates and (ii) the bottom layer, which is in direct contact with the $SiO_2$ substrate, might be too affected by disorder, spurious charges and concomitant localization to a point where most of the current would be effectively carried by the middle layer.[36] Here, our goal is to evaluate if such architecture would lead to an increase in the photogenerated electrical currents because the usefulness of the TMDs for high performance applications such as photodetectors, will likely depend on whether their current carrying capabilities can rival those of current silicon based devices/technologies.

Figure 4a displays the drain to source current $I_{ds}$ as a function of the bias voltage $V_{ds}$ under several values of illumination power from a $\lambda$ = 532 nm laser (spot size 3.5 um). This data


DOI: 10.1021/acsami.5b02264
ACS Appl. Mater. Interfaces 2015, 7, 12080–12088

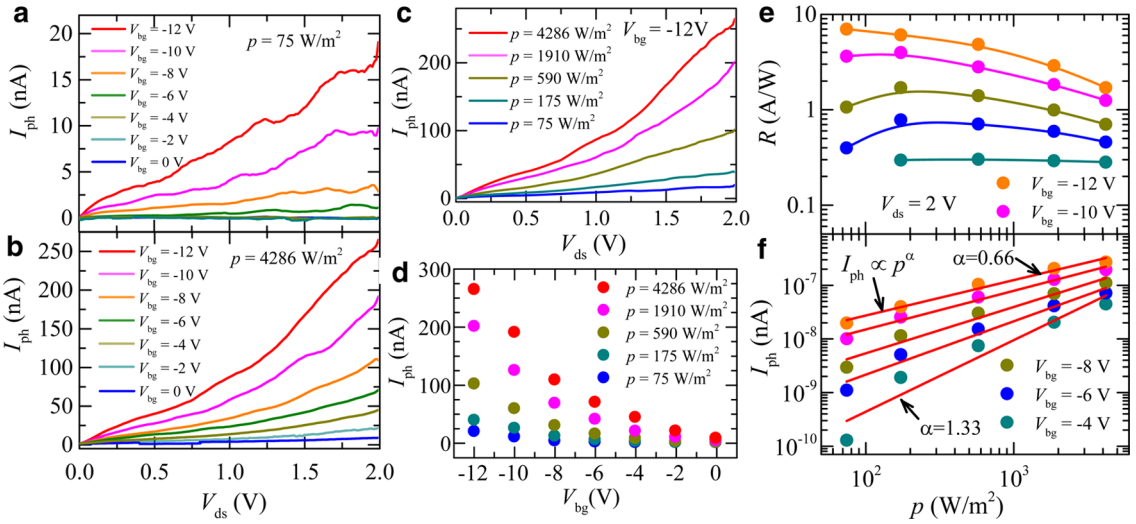


**Figure 5.** (a) Photocurrent $I_{ph}$ as a function of bias voltage $V_{ds}$ for a trilayered $WSe_2$ field effect transistor, for several values of the gate voltage $V_{bg}$ under a fixed optical power density $p$ = 75 W/m$^2$ (white light spectrum produced by a Xe lamp). These measurements were performed on the same sample whose photoresponse under $\lambda$ = 532 nm illumination is displayed in Figure 4. (b) Same as in panel a but for $p$ = 4286 W/m$^2$. (c) $I_{ph}$ as a function of $V_{ds}$ under a constant gate voltage $V_{bg}$ = −12 V and for several $p$ values. (d) $I_{ph}$ as a function of the gate voltage $V_{bg}$ for several $p$ values. (e) Photoresponsivity $R$ as a function of the white illumination power density $p$ under a bias voltage $V_{ds}$ = 2 V and for several values of the gate voltage $V_{bg}$. Notice the remarkably high $R$ values at low $p$. (f) $I_{ph}$ as a function of $p$ in a log−log scale, under $V_{ds}$ = 2 V and for several values of the gate voltage $V_{bg}$. Red lines are linear fits, i.e., $I_{ph} \propto p^{\alpha}$, yielding an exponent $\alpha$ ranging from ∼1.33 at low gate voltages to 0.66 at higher $V_{bg}$.

was collected in absence of gate voltage ($V_{bg}$ = 0 V). As seen, $I_{ds}$ displays a nonlinear dependence on $V_{ds}$ similarly to what was reported by ref 14 on $MoS_2$. The room temperature generated photocurrent, i.e., $I_{ph} = I_{ds}(P) - I_{ds}(P = 0)$, is the difference between the currents measured in dark condition (red trace) and under illumination. We did not detect significant time dependence for the photogenerated current once the laser light was turned on and kept at a constant power level. The resulting photoresponsivity $R$, which is the ratio between $I_{ph}$ and the applied illumination power $P$, is displayed in Figure 4b as a function of the excitation voltage $V_{ds}$, and for several values of $P$. As seen, the induced photocurrent increases considerably with increasing $P$. $R$ tends to display an asymmetric dependence on the sign of the excitation voltage $V_{ds}$ (see Figure S4 of the Supporting Information). As discussed in the Supporting Information, the origin of this asymmetry can be ascribed to the relative and nonintentional proximity of the laser spot to one of the current contacts. In effect, as discussed in detail in ref 20, the profile of the valence and conduction bands in TMDs changes considerably in the vicinity of the contact area due to the accumulation of charges induced by the Schottky barriers, particularly under the application of a bias voltage $V_{ds}$. The bias voltage further increases the local band bending and consequently it facilitates, under illumination, the promotion of charge carriers through the metallic contacts. In contrast, when $V_{ds}$ is reversed, the concomitant band bending becomes unfavorable for, for example, hole extraction or electron injection into the channel, thus decreasing the extracted photocurrent as experimentally seen. In ref 20, it is shown that most of the $I_{ph}$ is generated precisely at the interface between the channel and the electrical contacts where the electrostatic potential is found to be the strongest.

Nevertheless, the most important observation in Figure 4b is the size of the extracted photoresponsivity $R = I_{ph}/P$ in the absence of any gate voltage. $R$ approaches 150 mA/W at low $P$'s due to photogenerated currents ranging from $10^{-9}$ to $10^{-8}$ A; these values are similar to the ones reported in refs 16, 21, 23 and 37 for several TMDs. It is important to emphasize that the area of our conducting channel is nearly ∼27 times larger than the laser spot size, implying that the illumination of the entire channel (under the same power density) should increase the generated photocurrent by 1 order magnitude or even more. In Figure 4c, we plot the concomitant external quantum efficiency EQE, or the number of photogenerated carriers circulating through any given photodetector per adsorbed photon and per unit time, as a function of $V_{ds}$. Here, $EQE = hcI_{ph}/e\lambda P$, where $P$ is the illumination power irradiated onto the channel, $\lambda$ is the excitation wavelength, $h$ is Planck's constant, $c$ is the velocity of light and $e$ is the electronic charge. Notice how, in absence of gate voltages and under low illumination power, one can extract EQE values up to 40% under $P$ = 10 nW. However, as will be discussed below, the application of a small gate voltage, in the order of just $V_{bg}$ = −10 V, increases the value of $I_{ph}$ considerably indicating that it is possible to improve these values considerably by just varying the gate voltage or simply by increasing the bias voltage. Notice that these $R$ values are similar to those reported for multilayered $WS_2$;[37] although in ref 37, the illumination area is 58 $\mu$m$^2$, or approximately 6 times larger than our spot size, and $R$ was obtained under a considerably smaller power density. As will be subsequently demonstrated, by increasing the illumination area, under white light in this case, at a fixed power density, one can extract far more pronounced $R$ values, which in combination with appropriate values for $V_{bg}$ and $V_{ds}$ is likely to generate photocurrents approaching (or surpassing) $10^{-6}$ A. Again, we chose to limit the spot size of our laser beam to minimize the interaction with the contacts in an effort to evaluate the intrinsic photoresponsivity of $WSe_2$.

Figure 4d,e,f shows, respectively, $I_{ph}$, $R$ and the resulting EQE as a function of the laser illumination power $P$, under zero gate voltage, for two values of the bias voltage, $V_{ds}$ = +1 and +2 V, and for two crystals of similar thicknesses, i.e., sample #1 (black markers) and #2 (blue markers). In Figure 4d, the red line is a linear fit that yields $I_{ph} \propto P^{0.5}$. The nonlinear dependence of $I_{ph}$


DOI: 10.1021/acsami.5b02264
ACS Appl. Mater. Interfaces 2015, 7, 12080−12088

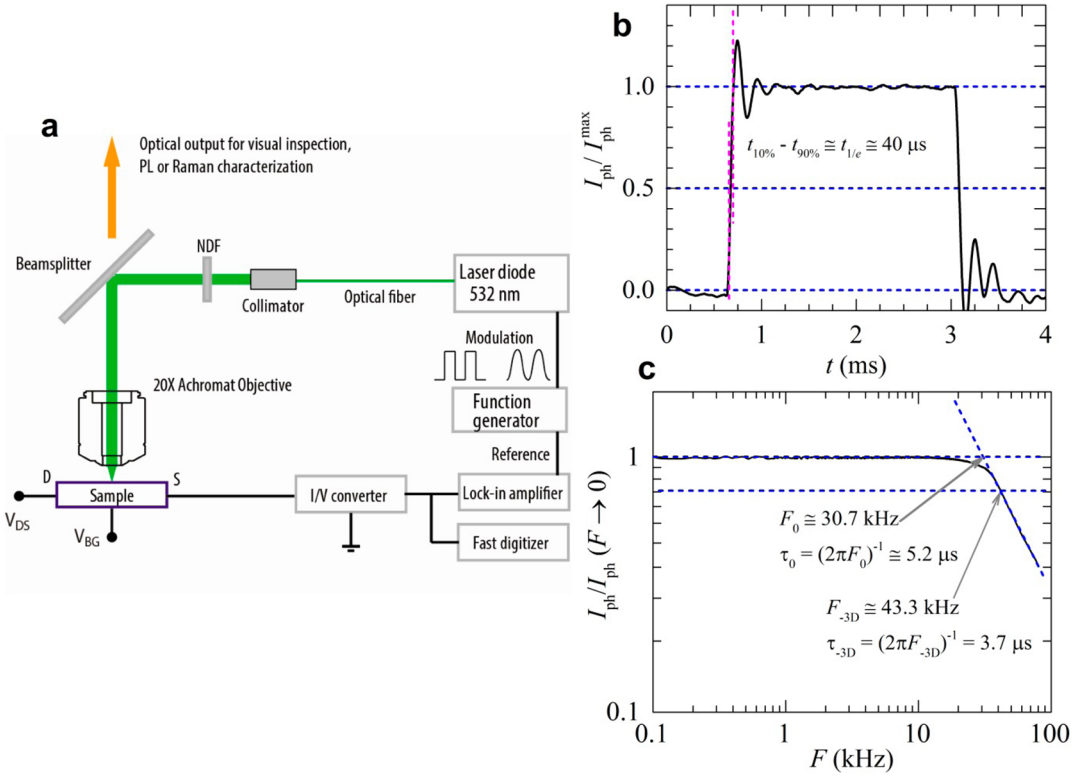


**Figure 6.** (a) Schematics of the experimental setup for measuring time dependent photoresponse. (b) Photogenerated signal (normalized by its maximum value) as a function of time in the dark and under 532 nm laser illumination under a modulation of 400 Hz, a laser power of 7.9 $\mu$W and measured at $V_{ds}$ = 1.5 V. The superimposed damped oscillatory component results from capacitive elements in the circuitry such as the gate capacitance. (c) Normalized photocurrent as a function of the laser modulation frequency.

on $P$ discards the photothermoelectric effect as the origin of the observed photoresponse. Notice how $R$ and EQE reach maximum values approaching ∼0.15 A/W and 40%, respectively, under a modest power of ∼10 nW, and for $V_{ds}$ = 1 V and $V_{bg}$ = 0 V. This $R$ value is ∼3 times larger than those extracted from CVD grown multilayered $WS_2$,[38] and from graphene−$WSe_2$ heterostructures.[39] It is higher or comparable to those extracted for multilayered $MoS_2$[16,18] despite the very small channel area illuminated by the laser beam, or the fact that the dependence of $R$ (or of EQE) on the excitation wavelength $\lambda$ has yet to be evaluated. As seen in Figure 4e, and similarly to what was reported by other groups,[14] the photoresponsivity decreases by more than 1 order of magnitude as $P$ increases. Most likely, this reflects the shortening of exciton recombination times as $P$ increases due to the concomitant increase in the density of photogenerated electron−hole pairs. Consequently, the external quantum efficiency as seen in Figure 4f, is observed to decrease as $P^{-0.5}$, reflecting the $P$-dependence of $I_{ph}$.

Now we proceed to evaluate the photoresponsivity of our trilayered $WSe_2$ phototransistor under the white light spectrum generated by a Xe lamp when it illuminates the entire channel. Figure 5a displays the photocurrent $I_{ph}$ as a function of the bias voltage, for several back gate voltages under a constant low illumination power density $p$ = 75 W/m$^2$. Figure 5b, on the other hand, shows $I_{ph}$ as a function of $V_{ds}$ under $p \cong$ 4.3 kW/m$^2$. Notice how an increase in $p$, by nearly 2 orders of magnitude, leads to an increase in $I_{ph}$ by just a little more than 1 order of magnitude. Figure 5c illustrates the evolution of $I_{ph}$ as a function of $V_{ds}$ on $p$ under a gate voltage $V_{bg}$ = −12 V. Figure 5d, on the other hand, plots $I_{ph}$ as a function of the gate voltage for several values $p$. As seen, $I_{ph}$ increases considerably as the value of the negative gate voltage increases. This reflects the progressive displacement of $V_{bg}$ toward the threshold gate voltage where the charges become fully delocalized (see Figure 2). Not surprisingly, this indicates that charge localization (see Figure S2 of the Supporting Information and related discussion) due to, for example, interface roughness is detrimental to the photoresponsivity of $WSe_2$. Figure 5e displays the photoresponsivity as a function of $p$ for several values of the gate voltage. Remarkably, at higher gate voltages and under the lowest values of $p$, which are far below the sunlight power density, one extracts $R$ values surpassing 7 A/W. More importantly, this value can be increased by increasing both the bias and the gate voltages. Such high $R$ values, when compared to the previous results collected under the $\lambda$ = 532 nm laser beam discussed in Figure 4, can be attributed to (i) a larger illumination area and (ii) to illumination of the area surrounding the contacts which is likely to contribute to the promotion of charge carriers across the Schottky barriers. Therefore, and although multilayered transition-metal dichalcogenides are characterized by an indirect band gap requiring the intervention of a phonon to generate an exciton, they are still characterized by pronounced photoresponsivities. Although, for our trilayered crystals excitons associated with the direct band gap are quite likely to play a major role in their photoresponse. In fact, this is further supported by Figure S3 of the Supporting Information, which shows the photoresponsivity of a 12-layer $WSe_2$ crystal indicating $R$ values surpassing 5 A/W at low power densities when collected under a bias voltage of just 0.1 V. In this sample, by increasing $V_{ds}$ to ∼1 V,


DOI: 10.1021/acsami.5b02264
ACS Appl. Mater. Interfaces 2015, 7, 12080−12088

as applied to the trilayered sample, one could increase $I_{ph}$ and the concomitant $R$ values, by at least 1 order of magnitude.

In Figure S5 of the Supporting Information, we show that the photoresponse of our trilayered $WSe_2$ FETs is frequency-dependent: shortening the excitation wavelength to $\lambda$ = 405 nm does not lead to an overall increase in their photoresponsivity, as one would expect from the observations in ref 14. In fact, it leads to a sharp decrease in $R$ and in the concomitant EQE due perhaps to excitation-dependent characteristic relaxation pathways with a predominant role for nonradiative decay.[40]

One important technological aspect for any potential photodetector is its characteristic temporal response. For example, single layer $MoS_2$ phototransistors displaying high photoresponsivities particularly at very low excitation powers,[14] displayed rather large characteristic response times, i.e., within several seconds.[14,17] But other groups reported a total photocurrent generation/annihilation time of just 50 ms.[18] To characterize the photoresponse dynamics of our trilayered $WSe_2$ FETs, we used two techniques: (i) ON/OFF light modulation to measure rise and fall time constants, (ii) AC sinusoidal modulation of the excitation light intensity to measure the characteristic response as a function of frequency. Figure 6 a shows a schematic of the experimental setup for measuring time dependent photoresponse. The laser diode output ($\lambda$ = 532 nm) was modulated through a function generator and controlled with a fast Si photodetector. The time-dependent generated photocurrent was converted into a time-dependent voltage, through an $I/V$ converter, and captured either by a digitizer, or by a Lock-In amplifier. The measurements were performed at $V_{bg} = -10$ V, implying that the FET is in its OFF state without light illumination. Figure 6b plots the photocurrent $I_{ph}$ measured as a function of time with turning the laser ON and OFF. The time constant $\tau_{ON/OFF}$ defined as the time required to change the signal amplitude between 10% and 90%, are about 40 $\mu$s for both rising and falling edges. Figure 6c shows the frequency dependence of the normalized photocurrent measured under sinusoidal light modulation, $I_{ph}(f)/I_{ph}$ $(f \rightarrow 0)$. The photocurrent begins to decrease beyond a characteristic roll over frequency $f_0$ = 30.7 kHz corresponding to a characteristic transient time $\tau_0 = (2\pi f_0)^{-1}$ = 5.2 $\mu$s. If instead one followed the bandwidth convention by choosing the frequency at which the photocurrent decreases by 3 dB, one would obtain $f_{3\ dB} \cong 43.3$ kHz corresponding to a characteristic time constant $\tau_{3\ dB} = (2\pi f_{3\ dB})^{-1} \cong 3.7$ $\mu$s. The current amplifier used in our setup is characterized by a rise time of 10 $\mu$s and a 3 dB bandwidth of 60 kHz corresponding to a time constant of 2.7 $\mu$s. Thus, the reported values $\tau_{ON/OFF} \cong 40$ $\mu$s and $\tau_{3\ dB} \cong 3.7$ $\mu$s represent a conservative estimate, implying that the actual photoresponse of these trilayered $WSe_2$ FETs is expected to be even faster. These values are comparable to the transient time constant of ~5 $\mu$s extracted for $SnS_2$ thin crystal arrays, which is claimed to be the fastest measured so far for transition metal dichalcogenides based phototransistors.[41] Also, it is important to emphasize that such short time constants discard any role for the photothermoelectric effect. The study in ref 23 suggests that the metallic contacts and concomitant Schottky barriers play a determinant role in the photoresponsive times of transition metal dichalcogenide phototransistors. Nevertheless, when using Ti for the electrical contacts, in photodetectors based on monolayer $WSe_2$, they obtain photoresponsive raise times of ~23 ms, or orders of magnitude higher than the photoresponsive times extracted here. This suggests that the interaction with the substrates is detrimental to the photoresponse times of transition metal dichalcogenides monolayers, hence justifying our choice of multilayered crystals.

## CONCLUSIONS

In summary, we have shown that few layer $p$-doped $WSe_2$ field-effect transistors built with the simplest possible architecture can display high carrier mobilities and a strong photocurrent response. This leads to a large photoresponsivity (e.g., ~7 A/W) and to remarkable external quantum efficiencies (e.g., 40%), surpassing those of Si photodetectors.[42] Most importantly, they also display fast photoresponse times ranging from a few $\mu$s to a few tenths of $\mu$s depending on the precise definition of the response time. Although much higher photoresponsivities were claimed for single layered $MoS_2$,[14] the values reported here surpass photoresponsivities and external quantum efficiencies extracted from more complex architectures which use graphene for the electrical contacts in heterostructures containing multilayered transition metal dichalcogenides.[39,43,44] In trilayered $WSe_2$, photoresponsivities $R > 7$ A/W under white light illumination and transient times ranging from ~4 to ~40 $\mu$s represent a good compromise between ref 14, which reports $R > 10^2$ A/W but with associated photoresponse times of a few seconds, and ref 41, which report transient times of 5 $\mu$s but with $R < 10$ mA/W.

We emphasize that there is still ample room for improvement of $WSe_2$ based phototransistors. Although our results do indicate that one is already able to extract sizable photocurrents, a systematic study on the thickness, spectral dependence, role of the electrical contacts and substrates, including bias- and gate-voltage dependences should lead to the extraction of even higher photocurrents than the values reported here, requiring the development of robust contacts. The important point is that the architecture implemented here is rather simple and does not require, for example, the use of dielectric engineering or the fabrication of van der Waals heterostructures,[39,43,44] which increase the complexity and therefore the production costs of potentially commercial phototransistors/photodetectors. Finally, our results are promising enough to justify a major engineering effort focused on increasing the carrier mobility, decreasing the channel and contact capacitances to shorten their characteristic photoresponsive times, and on increasing the carrier tunneling probability across the electrical contacts. If successful, this effort could unleash a new era in ultracompact, low power and perhaps even flexible optoelectronics.

## MATERIALS AND METHODS

$WSe_2$ single crystals were synthesized through a chemical vapor transport technique using either iodine or excess Se as the transport agent. Multilayered flakes of $WSe_2$ were exfoliated from these single crystals by using the micromechanical cleavage technique, and transferred onto $p$-doped Si wafers (with doping levels ranging from $2 \times 10^{19}$ to $2 \times 10^{20}$ $cm^{-3}$) covered with a 270 nm thick layer of $SiO_2$. For making the electrical contacts, 90 nm of Au was deposited onto a 4 nm layer of Ti via e-beam evaporation. Contacts were patterned using standard e-beam lithography techniques. After gold deposition, we proceeded with PMMA liftoff in acetone. The devices were annealed at 300 °C for ~3 h in forming gas, followed by high vacuum annealing for 24 h at 120 °C. Atomic force microscopy (AFM) imaging was performed using the Asylum Research MFP-3D AFM. Electrical characterization was performed by using a combination of sourcemeter (Keithley 2612A) coupled to a Physical Property Measurement System. The photoresponse was measured with a homemade micro-optical setup based on a modified microscope (Olympus BX51)


DOI: 10.1021/acsami.5b02264
ACS Appl. Mater. Interfaces 2015, 7, 12080−12088

enabling photocurrent, photoluminescence or Raman measurements. For photocurrent measurements under monochromatic illumination, we used a 532 nm solid-state CW laser (Coherent Sapphire 532-150 CDRH) or a 405 nm/532 nm laser diode system (Thorlabs DJ532-40, 532 nm; DL5146-101S, 405 nm; LTC100-A controller). The laser beam was injected into a single-mode optical fiber, delivered to a microscope sample stage through a 20× achromatic objective and focused into a spot of about 3.5 um in diameter. The incident optical power was adjusted with neutral density filters or by controlling the operating current of the laser diodes. The photocurrent was detected with and $I/V$ converter (DL1211 current amplifier). To measure the photoresponse times, the laser diodes were modulated using an external function generator while the photoresponse was measured with a high speed digitizer (NI PXI-5122) or a high-frequency lock-in amplifier (SRS SR844). A Xe lamp was used when performing measurements under white light. The incident illumination power was controlled by using neutral UV−vis filters placed between the lamp and the sample. An aperture was used to define a spot diameter of ∼9.3 mm. A broadband OPHIR-3A detector was used to measure the illumination power density.

## ■ ASSOCIATED CONTENT

### Supporting Information

Drain to source current as a function of back gate voltage for several temperatures, conductivity as function to the inverse of the temperature to the 1/3 power, indicating two-dimensional variable-range hopping conductivity, photocurrent data under white light for a 12-layer device, asymmetry of the photoresponse that is attributable to the interaction between carriers and light around the contact area, and photoconductivity, photoresponsivity and external quantum efficiencies for a shorter monochromatic wavelength. The Supporting Information is available free of charge on the ACS Publications website at DOI: 10.1021/acsami.5b02264.

## ■ AUTHOR INFORMATION


### Corresponding Authors

*L. Balicas. E-mail: balicas@magnet.fsu.edu.

*N. R. Pradhan. E-mail: pradhan@magnet.fsu.edu.


### Notes

The authors declare no competing financial interest.

## ■ ACKNOWLEDGMENTS

This work was supported by the U.S. Army Research Office MURI Grant No. W911NF-11-1-0362. J.L. acknowledges the support by NHMFL UCGP No. 5087. Z.L. and D.S. acknowledge the support by DOE BES Division under grant no. DE-FG02-07ER46451. The NHMFL is supported by NSF through NSF-DMR-1157490 and the State of Florida.

## ■ REFERENCES


(1) Novoselov, K. S.; Geim, A. K.; Morozov, S. V.; Jiang, D.; Zhang, Y.; Dubonos, S. V.; Grigorieva, I. V.; Firsov, A. A. Electric Field Effect in Atomically Thin Carbon Films. *Science* **2004**, *306*, 666−669.

(2) Dean, C. R.; Young, A. F.; Meric, I.; Lee, C.; Wang, L.; Sorgenfrei, S.; Watanabe, K.; Taniguchi, T.; Kim, P.; Shepard, K. L.; Hone, J. Boron Nitride Substrates for High-Quality Graphene Electronics. *Nat. Nanotechnol.* **2010**, *5*, 722−726.

(3) Novoselov, K. S.; Jiang, D.; Schedin, F.; Booth, T. J.; Khotkevich, V. V.; Morozov, S. V.; Geim, A. K. Two-Dimensional Atomic Crystals. *Proc. Natl. Acad. Sci. U. S. A.* **2005**, *102*, 10451−10453.

(4) Radisavljevic, B.; Radenovic, A.; Brivio, J.; Giacometti, V.; Kis, A. Single Layer $MoS_2$ Transistor. *Nat. Nanotechnol.* **2011**, *6*, 147−150.

(5) Larentis, S.; Fallahazad, B.; Tutuc, E. Field-Effect Transistor and Intrinsic Mobility in Ultra-Thin $MoSe_2$ Layers. *Appl. Phys. Lett.* **2012**, *101*, 223104.

(6) Chamlagain, B.; Li, Q.; Ghimire, N. J.; Chuang, H.-J.; Perera, M. M.; Tu, H.; Xu, Y.; Pan, M.; Xaio, D.; Yan, J.; Mandrus, D.; Zhou, Z. Mobility Improvement and Temperature Dependence in $MoSe_2$ Field-Effect Transistors on Parylene-C Substrate. *ACS Nano* **2014**, *8*, 5079−5088.

(7) Pradhan, N. R.; Rhodes, D.; Xin, Y.; Memaran, S.; Bhaskaran, L.; Siddiq, M.; Hill, S.; Ajayan, P. M.; Balicas, L. Ambipolar Molybdenum Diselenide Field-Effect Transistors: Field-Effect and Hall Mobilities. *ACS Nano* **2014**, *8*, 7923−7929.

(8) Fang, H.; Chuang, S.; Chang, T. C.; Takei, K.; Takahashi, T.; Javey, A. High-Performance Single Layered $WSe_2$ p-FETs with Chemically Doped Contacts. *Nano Lett.* **2012**, *12*, 3788−3792.

(9) Liu, W.; Kang, J.; Sarkar, D.; Khatami, Y.; Jena, D.; Banerjee, K. Role of Metal Contacts in Designing High-Performance Monolayer n-Type $WSe_2$ Field Effect Transistors. *Nano Lett.* **2013**, *13*, 1983−1990.

(10) Splendiani, A.; Sun, L.; Zhang, Y.; Li, T.; Kim, J.; Chim, C.-Y.; Galli, G.; Wang, F. Emerging Photoluminescence in Monolayer $MoS_2$. *Nano Lett.* **2010**, *10*, 1271−1275.

(11) Mak, K. F.; Lee, C.; Hone, J.; Shan, J.; Heinz, T. F. Atomically Thin $MoS_2$: A New Direct-Gap Semiconductor. *Phys. Rev. Lett.* **2010**, *105*, 136805.

(12) Lebegue, S.; Eriksson, O. Electronic Structure of Two-Dimensional Crystals from *ab Initio* Theory. *Phys. Rev. B* **2009**, *79*, 115409.

(13) Kuc, A.; Zibouche, N.; Heine, T. Influence of Quantum Confinement on the Electronic Structure of the Metal Sulfide $TS_2$. *Phys. Rev. B* **2011**, *83*, 245213.

(14) Lopez-Sanchez, O.; Lembke, D.; Kayci, M.; Radenovic, A.; Kis, A. Ultra Sensitive Photodetectors Based on Monolayer $MoS_2$. *Nat. Nanotechnol.* **2013**, *8*, 497−501.

(15) Zhang, W.; Huang, J.-K.; Chen, C.-H.; Chang, Y.-H.; Cheng, Y.-J.; Li, L.-J. High-Gain Photo Transistors Based on a CVD $MoS_2$ Monolayer. *Adv. Mater.* **2013**, *25*, 3456−3461.

(16) Choi, W.; Cho, M. Y.; Konar, A.; Lee, J. H.; Cha, G.-B.; Hong, S. C.; Kim, S.; Kim, J.; Jena, D.; Joo, J.; Kim, S. High-Detectivity Multilayer $MoS_2$ Phototransistors with Spectral Response from Ultraviolet to Infrared. *Adv. Mater.* **2012**, *24*, 5832−5836.

(17) Lee, H. S.; Min, S.-W.; Chang, Y.-G.; Park, M. K.; Nam, T.; Kim, H.; Kim, J. H.; Ryu, S.; Im, S. $MoS_2$ Nanosheet Phototransistors with Thickness-Modulated Optical Energy Gap. *Nano Lett.* **2012**, *12*, 3695−3700.

(18) Yin, Z.; Li, H.; Jiang, L.; Shi, Y.; Sun, Y.; Lu, G.; Zhang, Q.; Chen, X.; Zhang, H. Single Layer $MoS_2$ Phototransistor. *ACS Nano* **2012**, *6*, 74−80.

(19) Tsai, D.-S.; Liu, K.-K.; Lien, D.-H.; Tsai, M.-L.; Kang, C.-F.; Lin, C.-A.; Li, L.-J.; He, J.-H. Few Layer $MoS_2$ with High Broadband Photogain and Fast Optical Switching for Use in Harsh Environment. *ACS Nano* **2013**, *7*, 3905−3911.

(20) Wu, C.-C.; Jariwala, D.; Sangwan, V. K.; Marks, T. J.; Hersam, M. C.; Lauhon, L. J. Elucidating the Photoresponse of Ultrathin $MoS_2$ Field-Effect Transistors by Scanning Photocurrent Microscopy. *J. Phys. Chem. Lett.* **2013**, *4*, 2508−2513.

(21) Buscema, M.; Barkelid, M.; Zwiller, V.; van der Zant, H. S. J.; Steele, G. A.; Castellanos-Gomez, A. Large and Tunable Photoelectric Effect in Single-Layer $MoS_2$. *Nano Lett.* **2013**, *13*, 358−363.

(22) Monroy, E.; Omnès, F.; Calle, F. Wide-Bandgap Semiconductor Ultraviolet Photodetectors. *Semicond. Sci. Technol.* **2003**, *18*, R33−R51.

(23) Zhang, W.; Chiu, M.-H.; Chen, C.-H.; Chen, W.; Li, L.-J.; Wee, A. T. S. Role of Metal Contacts in High-Performance Phototransistors Based on $WSe_2$ Monolayer. *ACS Nano* **2014**, *8*, 8653−8661.

(24) Ando, T.; Fowler, A. B.; Stern, F. Electronic Properties of Two-Dimensional Systems. *Rev. Mod. Phys.* **1982**, *54*, 437−672.

(25) Pradhan, N. R.; Rhodes, D.; Zhang, Q.; Talapatra, S.; Terrones, M.; Ajayan, P. M.; Balicas, L. Intrinsic Carrier Mobility of Multilayer $MoS_2$ Field-Effect Transistor on $SiO_2$. *Appl. Phys. Lett.* **2013**, *102*, 123105.

(26) Chuang, H.-J.; Tan, X.; Ghimire, N. J.; Perera, M. M.; Chamlagain, B.; Cheng, M. M.-C.; Yan, J.; Mandrus, D.; Tománek, D.; Zhou, Z. High Mobility $WSe_2$ p- and n-Type Field-Effect Transistors




DOI: 10.1021/acsami.5b02264
*ACS Appl. Mater. Interfaces* 2015, 7, 12080−12088

Contacted by Highly Doped Graphene for Low-Resistance Contacts. *Nano Lett.* **2014**, *14*, 3594−3601.
(27) Wang, J. I-J.; Yang, Y.; Chen, Y.-A.; Watanabe, K.; Taniguchi, T.; Churchill, H. O. H.; Jarillo-Herrero, P. Electronic Transport of Encapsulated Graphene and $WSe_2$ Devices Fabricated by Pick-up of Prepatterned *h*-BN. *Nano Lett.* **2015**, *15*, 1898−1903.
(28) Podzorov, V.; Gershenson, M. E.; Kloc, Ch.; Zeis, R.; Bucher, E. High-Mobility Field-Effect Transistors Based on Transition Metal Dichalcogenides. *Appl. Phys. Lett.* **2004**, *84*, 3301−3303.
(29) Pradhan, N. R.; Rhodes, D.; Memaran, S.; Poumirol, J. M.; Smirnov, D.; Talapatra, S.; Feng, S.; Perea-Lopez, N.; Elias, A. L.; Terrones, M.; Ajayan, P. M.; Balicas, L. Hall and Field-Effect Mobilities in Few Layered $WSe_2$ Field-Effect Transistors. *Sci. Rep.* **2015**, *5*, 8979.
(30) Yang, H.; Heo, J.; Park, S.; Song, H. J.; Seo, D. H.; Byun, K.-E.; Kim, P.; Yoo, I.; Chung, H.-J.; Kim, K. Graphene Barristor, a Triode Device with Gate-Controlled Schottky Barrier. *Science* **2012**, *336*, 1140−1142.
(31) Das, S.; Chen, H.-Y.; Penumatcha, A. V.; Appenzeller, J. High Performance Multilayer $MoS_2$ Transistors with Scandium Contacts. *Nano Lett.* **2013**, *13*, 100−105.
(32) Lang, O.; Tomm, Y.; Schlaf, R.; Pettenkofer, C.; Jaegermann, W. Single Crystalline GaSe/$WSe_2$ Heterointerfaces Grown by van der Waals Epitaxy. II. Junction Characterization. *J. Appl. Phys.* **1994**, *75*, 7814.
(33) Lu, C.-P.; Li, G.; Mao, J.; Wang, L.-M.; Andrei, E. Y. Bandgap, Mid-Gap States, and Gating Effects in $MoS_2$. *Nano Lett.* **2014**, *14*, 4628−4633.
(34) Ghatak, S.; Pal, A. N.; Ghosh, A. Nature of Electronic States in Atomically Thin $MoS_2$ Field Effect Transistors. *ACS Nano* **2011**, *5*, 7707−7712.
(35) Qiu, H.; Xu, T.; Wang, Z.; Ren, W.; Nan, H.; Ni, Z.; Chen, Q.; Yuan, S.; Miao, F.; Song, F.; Long, G.; Shi, Y.; Sun, L.; Wang, J.; Wang, X. Hopping Transport through Defect-Induced Localized States in Molybdenum Disulphide. *Nat. Commun.* **2013**, *4*, 2642.
(36) Das, S.; Appenzeller, J. Where does the Current Flow in Two-Dimensional Layered Systems? *Nano Lett.* **2013**, *13*, 3396−3402.
(37) Lee, S. H.; Lee, D.; Hwang, W. S.; Hwang, E.; Jena, D.; Yoo, W. J. High Performance Photocurrent Generation from Two-Dimensional $WS_2$ Field-Effect Transistors. *Appl. Phys. Lett.* **2014**, *104*, 193113.
(38) Perea-López, N.; Laura, E. A.; Berkdemir, A.; Castro-Beltran, A.; Gutiérrez, H. R.; Feng, S.; Lv, R.; Hayashi, T.; López-Urías, F.; Ghosh, S.; Muchharla, B.; Talapatra, S.; Terrones, H.; Terrones, M. Photosensor Device Based on Few-Layered $WS_2$ Films. *Adv. Funct. Mater.* **2013**, *23*, 5511−5517.
(39) Britnell, L.; Ribeiro, R. M.; Eckmann, A.; Jalil, R.; Belle, V. D.; Mishchenko, A.; Kim, Y.-J.; Gorbachev, R. V.; Georgiou, T.; Morozov, S. V.; Grigorenko, A. N.; Geim, A. K.; Casiraghi, C.; Castro Neto, A. H.; Novoselov, K. S. Strong Light-Matter Interactions in Heterostructures of Atomically Thin Films. *Science* **2013**, *340*, 1311−1314.
(40) Kozawa, D.; Kumar, R.; Carvalho, A.; Amara, K. K.; Zhao, W.; Wang, S.; Toh, M.; Ribeiro, R. M.; Castro Neto, A. H.; Matsuda, K.; Eda, G. Photocarrier Relaxation Pathway in Two-Dimensional Semiconducting Transition Metal Dichalcogenides. *Nat. Commun.* **2014**, *5*, 4543.
(41) Su, G.; Hadjiev, V. G.; Loya, P. E.; Zhang, J.; Lei, S.; Maharjan, S.; Dong, P.; Ajayan, P. M.; Lou, J.; Peng, H. Chemical Vapor Deposition of Thin Crystals of Layered Semiconductor $SnS_2$ for Fast Photodetection Application. *Nano Lett.* **2015**, *15*, 506−513.
(42) Kasap, S. O. *Optoelectronics and Photonics: Principles and Practices*; Prentice-Hall, Inc: Upper Saddle River, NJ, 2001.
(43) Yu, W. J.; Liu, Y.; Zhou, H.; Yin, A.; Li, Z.; Huang, Y.; Duan, X. Highly Efficient Gate-Tunable Photocurrent Generation in Vertical Heterostructures of Layered Material. *Nat. Nanotechnol.* **2013**, *8*, 952−958.
(44) Lee, C.-H.; Lee, G.-H.; van der Zande, A. M.; Chen, W.; Li, Y.; Han, M.; Cui, X.; Arefe, G.; Nuckolls, C.; Heinz, T. F.; Guo, J.; Hone, J.; Kim, P. Atomically Thin p−n Junctions with van der Waals Heterointerfaces. *Nat. Nanotechnol.* **2014**, *9*, 676−681.


DOI: 10.1021/acsami.5b02264
*ACS Appl. Mater. Interfaces* 2015, 7, 12080−12088